

Systematic review of pre-clinical and clinical devices for magnetic resonance-guided radiofrequency hyperthermia

Fatemeh Adibzadeh, Kemal Sumser, Sergio Curto, Desmond T. B. Yeo, Amir A. Shishegar & Margarethus M. Paulides

To cite this article: Fatemeh Adibzadeh, Kemal Sumser, Sergio Curto, Desmond T. B. Yeo, Amir A. Shishegar & Margarethus M. Paulides (2020) Systematic review of pre-clinical and clinical devices for magnetic resonance-guided radiofrequency hyperthermia, International Journal of Hyperthermia, 37:1, 15-27, DOI: [10.1080/02656736.2019.1705404](https://doi.org/10.1080/02656736.2019.1705404)

To link to this article: <https://doi.org/10.1080/02656736.2019.1705404>



© 2020 The Author(s). Published with license by Taylor & Francis Group, LLC



Published online: 09 Jan 2020.



Submit your article to this journal [↗](#)



Article views: 361



View related articles [↗](#)



View Crossmark data [↗](#)

Systematic review of pre-clinical and clinical devices for magnetic resonance-guided radiofrequency hyperthermia

Fatemeh Adibzadeh^{a,b*}, Kemal Sumser^{a*} , Sergio Curto^a, Desmond T. B. Yeo^c, Amir A. Shishegar^b and Margarethus M. Paulides^{a,d}

^aDepartment of Radiation Oncology, Erasmus MC – Cancer Institute, University Medical Center Rotterdam, Rotterdam, The Netherlands;

^bDepartment of Electrical Engineering, Technical University of Sharif, Tehran, Iran; ^cGE Global Research, Niskayuna, NY, USA; ^dDepartment of Electrical Engineering, Technical University of Eindhoven, Eindhoven, The Netherlands

ABSTRACT

Clinical trials have demonstrated the therapeutic benefits of adding radiofrequency (RF) hyperthermia (HT) as an adjuvant to radio- and chemotherapy. However, maximum utilization of these benefits is hampered by the current inability to maintain the temperature within the desired range. RF HT treatment quality is usually monitored by invasive temperature sensors, which provide limited data sampling and are prone to infection risks. Magnetic resonance (MR) temperature imaging has been developed to overcome these hurdles by allowing noninvasive 3D temperature monitoring in the target and normal tissues. To exploit this feature, several approaches for inserting the RF heating devices into the MR scanner have been proposed over the years. In this review, we summarize the status quo in MR-guided RF HT devices and analyze trends in these hybrid hardware configurations. In addition, we discuss the various approaches, extract best practices and identify gaps regarding the experimental validation procedures for MR - RF HT, aimed at converging to a common standard in this process.

ARTICLE HISTORY

Received 19 April 2019
Revised 23 November 2019
Accepted 10 December 2019

KEYWORDS



MR temperature imaging;
noninvasive thermometry;
MR-guided radiofrequency
hyperthermia; hybrid
hardware configurations;
qualitative and quantitative
validations

Introduction

Hyperthermia (HT) treatments involve heating tissues to the range of 40–44 °C for 60–90 min [1]. The majority of the HT treatments are applied using external devices employing radiofrequency (RF) electromagnetic waves [2,3]. Clinical trials have shown that RF HT improves clinical outcome, without adding to the toxicity, of radiotherapy and a number of chemotherapies [4–6]. Clinical work showed that intra-tumoral temperatures are correlated with clinical outcome parameters such as local control of tumors [7–15]. Due to the body's strong, inhomogeneous and variable thermoregulation [16–19], close monitoring of the temperature is required to optimize the power distribution accordingly. Here, the goal is to focus energy at the target region and prevent unwanted hotspots in normal tissues. Several different approaches for noninvasive thermometry, like impedance tomography, active and passive microwave imaging, CT, laser, infrared, ultrasound, MR-techniques, have been investigated in the last decades. Among all these different techniques, MR thermometry (MRT) has been elaborated most extensively and validated in clinical and experimental settings [20,21]. In addition, the gantry of the current MRI systems provides the possibility for mechanical integration with hyperthermia applicators [22]. MR imaging also provides the possibility to

image the complete treatment setup, i.e., patient surrounded by the applicator, as well as monitoring perfusion/tissue cooling and the response to treatment. To enable all the aforementioned benefits of using MRI with RF hyperthermia devices, the compatibility of these devices with the MRI system ('MR compatibility') is crucial, especially in terms of how they impact image quality. These properties are often not quantified and reported in a standardized way for interventional devices. An overview of such systems and an inventory of the required image quality metric is, however, currently lacking.

The important potential benefits of noninvasive thermometry can be highlighted best when compared to invasive thermometry, which is the current golden standard for intra-tumoral temperature assessment during RF HT therapy. In invasive thermometry, temperature probes are inserted into closed-tip catheters and placed in body cavities or pierced into tissue. Invasive thermometry can be done using commercially available types of thermocouples and thermistors suitable for use in clinical hyperthermia. Available thermistors are the Bowman thermistor probe [23] (BSD Medical Corp., Salt Lake City, UT) and the fiber-optic (FISO) thermistor probe (gallium arsenide (GaAs) [24] and fluorescence (fluoroptic) [25] probes). Thermocouples and the Bowman thermistor probes rely on detection of a voltage and fiber-optic probes

CONTACT Kemal Sumser  k.sumser@erasmusmc.nl  Department of Radiation Oncology, Erasmus MC – Cancer Institute, University Medical Center Rotterdam, Rotterdam, The Netherlands

*These authors contributed equally to this work.

© 2020 The Author(s). Published with license by Taylor & Francis Group, LLC

This is an Open Access article distributed under the terms of the Creative Commons Attribution License (<http://creativecommons.org/licenses/by/4.0/>), which permits unrestricted use, distribution, and reproduction in any medium, provided the original work is properly cited.

rely on the temperature dependency of band gap and refraction index. The reported accuracy of the fiber-optic and bowman probes are better than $\pm 0.1^\circ\text{C}$ and $\pm 0.2^\circ\text{C}$, respectively, taken from datasheets by the manufacturer. Although accurate, such thermometry provides very limited spatial information, i.e., only along the line of the catheter. Specifically, for RF HT treatment where a large volume is heated, the probability that invasive thermometry detects all the hotspots of interest is low. This is due to the limited number of temperature probes, and clinical restrictions for placement of thermometry catheters. In addition, probe insertion may be painful and hazardous. Complications such as infection or neurological complaints and other discomfort were observed along with a low acceptance in patients and physicians [26,27]. Therefore, MRT has the potential to replace the invasive thermometry in the clinic because of its noninvasive nature, high spatial resolution and 3-dimensional (3D) anatomical coverage per unit time.

The first decade after the advent of MRT was devoted to developments in techniques allowing temperature assessment during thermal therapies [28–32]. Several temperature-sensitive parameters were studied, like the proton-resonance frequency shift (PRFS), apparent diffusion coefficient (ADC), longitudinal relaxation time (T1), transversal relaxation time (T2), and equilibrium magnetization (M0) [33–35]. Of these endogenous temperature indicators, techniques that leverage the PRFS effect observed in water-rich tissue have been studied more extensively [33,34,36]. This technique is based on the fact that the change in image phase in a pair of gradient echo images acquired at two different temperatures is linearly proportional to the temperature change. This arises from a proton resonance frequency that linearly decreases as temperature increases in the water molecule ($-0.01\text{ ppm}/^\circ\text{C}$) [37]. The second decade saw the development of techniques that enabled more robust and reliable results, especially for *in vivo* applications [38–41]. However, the PRFS effect is small and, thus, is highly sensitive to magnetic field perturbations, which degrade MR thermometry accuracy. Such degradation is especially pronounced in long duration hyperthermia treatments ($\sim 90\text{ min}$). These magnetic field perturbations may be caused by a number of possible mechanisms that manifest themselves differently. For example, gradient-induced heating of passive shim elements may cause non-periodic temporal B0 drift that vary smoothly in space across the imaging field-of-view, while patient respiratory/cardiac motion may induce periodic B0 perturbations in a local region, especially near interfaces of tissues that have different magnetic susceptibility values. Non-periodic and local B0 perturbations may also arise from intestinal/bowel movement. The removal of these temporal field perturbation effects is crucial for successful MRT for radiotherapy monitoring, and the different variants of B0 perturbation may require different types of correction methods. The inherent signal-to-noise-ratio (SNR) of MR signals is another very important quantity that impacts the accuracy and robustness of MRT.

For MR-guided radiofrequency hyperthermia (MRgRFHT), the RF body coil in the MRI scanner is typically used to receive MR signals for MRT since HT devices are not

designed to allow the concurrent placement and use of commercial MR flexible coils. Hence, the SNR available is relatively low since the RF body coil is positioned much further from the region of interest (ROI) compared to a surface coil array that could have been placed in close proximity to the patient. Moreover, RF body coils in commercial MRI scanners can only receive MR signals in single (quadrature) channel mode and thus do not exploit parallel imaging for scan time reduction. To address this problem, new hardware designs are being researched to improve SNR and enable MR parallel imaging, while simplifying and reducing equipment footprint (physical space that a device occupies). This can increase the reliability of MR-temperature measurements and improve patient access to MRgRFHT in the clinic.

The purpose of this paper is to analyze all research work done in the space of MRgRFHT, and review the status in terms of device validation, preclinical investigations and clinical trials. In this analysis, we excluded papers on devices aimed at thermal ablation and those focused on MR thermometry techniques and algorithms. The current review attempts to review the scope of technical advances in MRI guided RF HT for new scientists, clinicians and other professionals and provide the groundwork for improved validation by summarizing and proposing standards on its reporting.

Materials and methods

We performed a literature search in the Scopus and the Web of Science (WoS) databases using the following search strings:

TITLE-ABS-KEY [((((*'magnetic resonance'* OR *mr*) AND *thermometry*) OR *'thermal magnetic resonance'* OR *'thermal mr'* OR *'temperature imaging'*) AND *'hyperthermia'*

OR

TITLE-ABS-KEY (*hyperthermia* AND *mri*) AND (*clinical* OR *preclinical*) AND (*evaluation* OR *validation* OR *verification*)

AND

TITLE-ABS-KEY (*hybrid* OR *integrated* OR *hardware* OR *configuration* OR *setup* OR *'set-up'* OR *system* OR *device* OR *applicator* OR *prototype* OR *platform*)

where TITLE-ABS-KEY indicate either the title, abstract or keywords of the paper. This resulted in 325 articles (249 in Scopus and 76 WoS). The duplicated results in the two databases were removed. We further added 4 articles that were not found in the structured literature search and 2 conference abstracts that were not available in the Scopus or WoS databases.

Two exclusion steps were then introduced for selecting only papers concerning RF-HT (exclusion criterion 1) and original papers (exclusion criterion 2). The selection process is summarized in Figure 1.

In exclusion criterion 1, all papers were excluded having TITLE-ABS-KEY on the following:

- Ablation
- Non-RF HT, e.g., HIFU/Laser studies
- Methodology, algorithm (e.g., theory of temperature monitoring and resolution, evaluation of temporal spatial

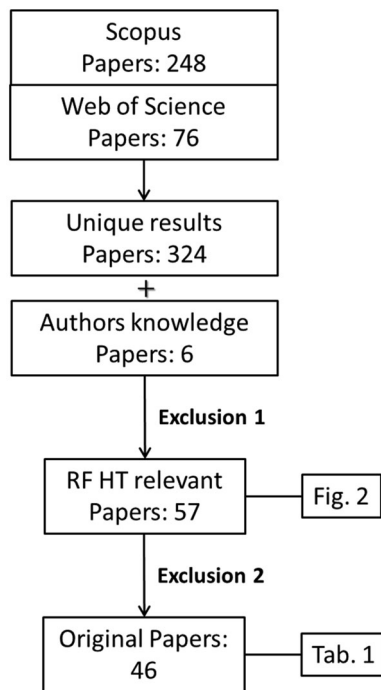


Figure 1. Selection process for inclusion of papers with criteria reported in the text.

resolution, estimation and correction of induced errors due to breath or organ displacement (motion)).

Application of exclusion criterion 1 reduced the number of papers to 106 articles (85 Scopus 19 WoS and 2 conference abs) after reading title-abstract and to 57 articles (46 Scopus, 9 WoS, and 2 conference abstracts) after reading the full text. This selection comprised the relevant papers on MR guided RF-only HT devices.

Exclusion criterion 2 intended to only include original studies which presented novel design and prototypes. Articles including the following were excluded:

- Review articles
- Non-English language articles
- Book series or only insufficient abstracts available

After exclusion criterion 2, 46 papers (39 Scopus, 5 WoS, and 2 conference abstracts) remained presenting or investigating novel hybrid MRgRFHT devices. These devices are categorized in the next section and summarized in Table 1. In this work, we defined quantitative validation as the agreement between the measured quantities in MRT versus a gold standard technique, e.g., average error between MRT and invasive probe measurements. Those papers reporting only the quality of the agreement as an impression or distribution, i.e., quantifying only the shape and size of the heated zones in the MR images, were scored as qualitative.

MR-guided RF HT devices

Various approaches aiming to integrate RF-HT applicators and MRI system have been proposed and can be roughly

categorized into (1) decoupled systems (HT-only inserts); (2) integrated systems (Dual-function inserts).

Decoupled devices (HT-only inserts)

These devices are based on an independent RF transmission chain and an RF-HT applicator insert that operates inside the bore of a MRI scanner. Since such hyperthermia devices operate independently from the MR system, heating and imaging can be performed simultaneously. Unless mentioned otherwise, the MRI scanner's RF body coil is used for both RF transmit and receive of the MR signals. Such developed devices are:

Noninvasive clinical setups

– *BSD2000-3D-MRI* applicator is the only MR-guided RF HT device that has led to a commercial prototype, in combination with 1.5T MRI systems. This applicator consists of 12 dipole antenna pairs operating at 100 MHz, arranged on three rings of four dipole pairs each, that are independently controlled to steer the energy focus toward deep seated tumor volumes. This device has been validated both preclinically [40,42–44] and clinically [45,46]. A systematic comparison of 3D-specific absorption rate (SAR) distribution between MRT and planning calculations in a homogenous cylindrical and heterogeneous elliptical phantom demonstrated a deviation in the range of 2–3 W/kg, i.e., below 10% [43]. The possibility to adapt/optimize SAR pattern in a phantom by employing MR thermometry in an iterative procedure were also shown for this applicator [47]. A recent more systematic quality assurance analysis of this system in a 1.5T MRI scanner showed a mean maximum temperature increase ($T_{\text{increase, max}}$) in a Perfax homogeneous phantom of $5.9 \pm 0.4^\circ\text{C}$, using 1000 W input power for 12.4 min, and a mean steering error of $0.4 \pm 0.2\text{ cm}$ [44]. Clinical experiments in 15 patients [46] with pre-irradiated rectal recurrences showed significant correlation between the MRT-derived mean temperatures in the tumor with invasive measurements, tumor features (volume and location) and clinical response ($p = 0.04$) [46].

– The mini-annular-phased array (MAPA) RF HT applicator is the only other applicator which has been used on patients. The MAPA consists of four pairs of flared dipole antennas and was designed to treat limb tumors in extremities and modified for insertion into MRI scanner [48]. Usually a single frequency (140 MHz) and signals of equal amplitude and phase have been used. Hybrid operation was validated by inserting the MAPA into a 0.5T whole body MRI system and its head coil during synchronous heating and imaging [32,48,49]. In these studies, diffusion coefficient based temperature imaging methods were used to monitor temperatures in a gel based phantom. Temperatures in 1 cm^2 regions of interest were found to be within 0.2°C from invasive measurements. Clinical validation was performed in 4 patients with high-grade primary sarcoma tumors of the lower leg [50] and 10 patients with high grade extremity soft tissue sarcomas [51]. On the tumor ROIs, the mean difference

between PRFS-MRT and interstitial point measurements was 0.62°C in steady state.

- The *MRlabCollar* is an MR-compatible laboratory prototype of the HYPERcollar3D HT applicator consisting of two rings of six patch antennas operating at 434 MHz. Pilot measurements by Numan et al. (2013) using the lower half of the original LabCollar showed an average PRFS-MRT accuracy of 0.4°C ($0.1\text{--}0.7^{\circ}\text{C}$) against fiber-optic probe thermometry [52]. Heating size and shape had a good correlation with predictions ($R^2 = 0.76$). Paulides et al. (2014) introduced the design of an MR compatible head and neck laboratory prototype applicator and showed the focused heating capabilities of MRlabcollar [53]: a maximum SAR of 100 W kg^{-1} and a temperature increase of 4.5°C in 6 min was feasible using 300 W input power in a cylindrical fat/muscle phantom. The central heated region in this phantom corresponded very well to those obtained earlier by infrared measurements in a muscle-only split-phantom phantom for the setup without MR compatibility feature (LabCollar) [54]. This device was again validated pre-clinically in an oil-gel phantom by applying a combination of MR imaging and 3D spline fitting for accurate probe localization [55]. The result corresponds to a reduced average error of $\Delta T < 0.14^{\circ}\text{C}$ with a maximum error of $\Delta T = 0.22^{\circ}\text{C}$.

- The *MRCollar*, the clinical implementation of the MRlabcollar, consists of 12 dielectric parabolic reflector antenna (DIPRA) modules, i.e., parabolic water-filled encasings around printed reflector-backed dipole antennas [56]. Two arrays of six antenna structures were placed in two semi-circular structures. By electromagnetic simulations, the authors showed that the power focusing ability of the device in terms of the target coverage of the 25% iso-SAR contour (TC25) is $83.7 \pm 15.6\%$ for head and neck tumors in clinic. A reduced scale phantom experiment demonstrated that only very localized image distortion was observed. MR imaging was obtained using the body coil of 1.5 T MRI scanner.

- *Capacitive*: a two-channel capacitive RF heating system, consisting of four electrodes operating at 26 MHz, was evaluated on a phantom aiming to heat a deep-seated target region in which electrical conductivity was elevated by nanoparticle mediation [57,58]. When one electrode pair was activated, the other electrode pair was electrically isolated to prevent RF current leakage between the electrodes. MRT, using a 3 T MRI sequentially with the RF heating, showed maximum $\Delta T_{\text{ave}} < 0.5^{\circ}\text{C}$ relative to fiber-optic measurements after phase error correction in the center of the phantom. Using this system, Hernandez et al. (2016) proposed a correction method of B0 drift effects in MR thermometry [59], for which they placed magnetic field monitoring (MFM) probes around the subject to compute phase correction maps for MRT by interpolating the center frequencies of MFM signals on the imaging slice. Using phantom measurements, the authors showed that this B0 drift correction reduced the mean squared temperature error of MR thermometry to an average of 0.47°C . This device is the only capacitive MR guided RF HT device and the only system that used MFM probes instead of fat references for B0 field drift corrections.

- The current sheet antennas (CSA) is a phased array consisting of two identical MR-compatible current sheet antennas operating at 100 MHz. Hoffmann et al. (2002) used CSA for heating a tissue-equivalent phantom inside a 3 T MRI [60]. The heating capabilities were measured with PRFS method in sequential heating and imaging experiments. The maximum error between the MR-derived and fiber-optic measured temperatures was estimated to be $\pm 1^{\circ}\text{C}$ and the SD was 0.4°C . This development has not translated into a clinical product.

- The clinical WACOA applicator (CWA) is a HT applicator consisting of 12 separate Water COated Antenna (WACOA) modules operating within a 1.5 T MRI scanner. The modules are designed as MR-compatible, specially shaped and adjustable, cylindrical dipole structures embedded into hermetically closed cassettes filled with deionized water. Experimental and numerical evaluations demonstrated that the CWA is able to steer the 3D temperature pattern [61]. In 2005, the device was evaluated by a 3D comparison of predicted and measured temperature data sets for an inhomogeneous phantom [62]. The average error of the calculated versus measured temperature comparison was 0.45°C . CWA was the first device which had its numerical model validated with 3D MR-temperature measurements, but it was not translated into a clinical version.

- The *hexagonal flared-type* whole body phased array applicator operates at 130 MHz and consists of 3 pairs of flared dipole antennas. The root mean square (RMS) and average difference between the MR-derived temperatures (1.5 T) and probe temperatures in phantom were 1.23°C and 0.92°C , respectively [63]. The standard error of the mean temperature change was found to be 0.22°C in a 50 mm^3 region of a gel phantom for echo time of 20 ms [64]. The group also performed *in vivo* experiments to evaluate the ability of MRT in canine brain and muscle [64–66]. The results showed a standard error of 0.6°C in a 16 mm^3 volume for brain tissue and muscle tumor (sarcoma) [64].

Invasive clinical setups

- The *intravascular MRI guidewire* is an interstitial system that simultaneously produces RF heating and high SNR imaging/temperature mapping used for enhancement of vascular gene transfer. The system consists of MRI guidewire placed within the guidewire channel of a gene delivery catheter and is connected to an 1.5 T MR scanner and external RF generator/amplifier through a filter box [67]. The system was validated both *in vitro* (cylindrical phantom, qualitative validation) and *in vivo* (in the aorta of rabbits). For the *in vivo* experiment, the SD error between the MR-derived temporal curve and that of the fiber-optic measured temperature curve was 1.2°C . Moreover, the maximum temperature increase in target aortic wall was approximately 7°C from a baseline temperature of 37°C using 4–5 W input power for about 4 min. The intravascular MRI guidewire was the first device that used the same antenna for RF heating and MR imaging in a simultaneous operation.

Preclinical (animal) setups

Preclinical setups are small and flexible in comparison to conventional HT systems and generally combined with ultra-high field preclinical MRI systems. The antennas predominantly operate at 2.45 GHz.

- The *Slot&Dipole applicator* by Demura et al. (2006) are two MR-compatible microwave applicators operating at 2.45 GHz of dipole-type and slot-type and evaluated using phantoms and living animals [68]. A 10-mm-deep area could be heated at an average target temperature of $42.60 \pm 0.14^\circ\text{C}$ and a skin surface temperature of $43.27 \pm 0.45^\circ\text{C}$, using 60–110 W input power intermittently (2 s power-on, 2 s power-off) for 60 min experimental period. The 95% limits of agreement between MR and fluoroptic thermometry in the three rabbits were $+0.318/-0.339^\circ\text{C}$, $+0.693/-0.661^\circ\text{C}$, and $+0.564/-0.526^\circ\text{C}$, respectively.

- The *coaxial* applicator incorporates a 3.5 mm directional microwave antenna operating at 2.45 GHz designed for small animal investigations inside the 30 mm bore of the 14 T ultra-high field MRI scanner [69]. Simulations and experiments in tissue mimicking phantoms demonstrated the feasibility of heating $21\text{--}982\text{ mm}^3$ targets to temperature rises of $T_{\text{increase}} > 3^\circ\text{C}$ at radial distances up to $\sim 6\text{ mm}$ from the applicator, with 8–12 W input power. ΔT_{max} between MR thermometry and fiber-optic temperatures was $\leq 0.6^\circ\text{C}$. *In vivo* experiments demonstrated the feasibility of delivering HT to implanted tumors in two experimental mice in combination with PRFS based MRT [69]. $\sim 4^\circ\text{C}$ and $\sim 11^\circ\text{C}$ temperature increase were achieved with 20 W microwave exposure for 5 min and 15 min, respectively.

- The *Yagi-Uda-based* small animal HT applicator operating at 2.45 GHz was designed and validated by Raaijmakers et al. (2018) for superficial HT in small animals in a 7 T MR scanner [70]. The antenna was based on an earlier designed MR-compatible Yagi-Uda antenna presented by Paulides et al. (2017) [71]. The antenna was designed for a low MR-footprint and directional radiation properties to minimize inter-element coupling for typical array configurations ($S_{21} < -23\text{ dB}$). Validation in a homogenous muscle phantom showed PRFS-MRT to correlate with temperature probe measurements (root mean square error: $\text{RMSE} = 0.51^\circ\text{C}$ and $R^2 = 0.99$) and the ability to create a small heating focus ($< 1\text{ cm}^3$) in an animal-sized muscle-mimicking phantom. The applicator was mechanically redesigned by reducing the distance between antenna arms and the target [72] to reduce losses in the deionized water (severe at 2.45 GHz) between antenna and animal. *In vivo* experiments in leg tumors of four nude mice showed a ΔT of 7°C in 5 min using 7 W power and no artifacts were observed in the MR images during simultaneous heating and imaging.

- The Annular-phased Array (APA) is composed of six dipole antennas for heating deep seated regions of the body. Kowalski et al. (2002) proposed a phase/amplitude optimization technique using only information from MRT [73]. Preclinical validation of the device, operating at 915 MHz, was performed by heating a homogeneous cylindrical phantom [73,74]. The applicator and phantom were placed inside an MRI birdcage coil, and the entire assembly

was inserted into a 4.7 T MRI magnet. Fluoroptic probe measurements demonstrated control of the heat focus position employing only MRT-based temperature feedback information. The APA is the only applicator where the ultimate goal of MRgRFHT, i.e., control of the temperature distribution based on MRT, was realized during a phantom heating experiment.

Dual-function devices

These devices use the same antenna array for heating and imaging. When the MRI RF body coil is used for imaging, problems such as inter-system cross-talk, signal oscillations and low image SNR arises. Dual-function devices overcome these limitations since they only have a single system, they have multichannel antenna operation and the antennas are closer to the target for higher signal pickup. However, since these devices require interleaved operation, simultaneous operation cannot occur.

Electronic switching

These devices consist of a single set of conductive structures that can alternately be used for MRI receive and RF heating using fast electronic switches. The two possible implementations use either the scanner's RF transmit chain for heating at the Larmor frequency or a separate transmit chain to apply RF energy at a different frequency. Inter-system coupling and RF HT equipment footprint is theoretically smaller in such devices compared to decoupled two-system configurations. Yeo et al. (2011) introduced one such device operating at 128 MHz (Larmor frequency at 3 T), which switches between a loop coil array for MR imaging and a C-shaped dipole antenna array that generates focused electric fields for RF heating *via* selective inclusion/exclusion of impedance matching and tuning capacitors using fast RF switches [75]. The results indicated that C-shaped dipole antenna arrays can induce steerable heating similar to straight dipole antenna arrays. The loop coil array functions as a 3 T MRI RF receiver that yields an imaging SNR that is about three times higher than that of an RF body coil. Therefore, C-shaped dipole antenna arrays could potentially enable 3D heat steering and MRI with the same physical hardware.

Thermal MR

Another approach, designated as 'thermal MR', allows RF heating and MR imaging application using the same antenna array and the power amplifier of the MR system. Here, part of the regular imaging sequence time, e.g., the last 10%, is used to apply RF for heating. This approach is particularly effective in MR scanners at ultra-high magnetic fields ($\geq 7\text{ T}$) for which the Larmor frequency approaches the optimum frequency for semi-deep heating [76,77]. The advantage of the pulse modulated signal used for RF HT and MRT is the ability to modify the imaging technique in order to perform RF HT and MRI at the same frequency without the need for electronic switching which further reduces the dead time for

contemporaneous operation. In addition, the electric fields for imaging and heating are equal, thus, *in vivo* quality assurance can be applied using B1+ imaging as a surrogate for the electric field induced in the patient. One such device is an 8-channel transmit/receive (Tx/Rx) hybrid RF applicator consisting of bow-tie dipole antennas ('dual function bowtie array') that generate an E-field pattern for RF heating and a circular polarized H-field for MRI [76]. Each channel has independent control of phase and amplitudes. The applicator was connected to the MR system *via* a coil interface comprising 8 Tx/Rx switches.

In 2015, Winter et al. presented the preclinical results derived from the same applicator at 300 MHz using a cylindrical phantom mimicking brain tissue with the size of a human head [77]. The experiments demonstrated that the pulsed multi-channel transmit system of a 7 T MR scanner supports targeted RF heating and provides enough power ($P_{\text{avg}} > 400 \text{ W}$) to induce a temperature increase of $\sim 11^\circ\text{C}$ in 3 min in the center of a head sized phantom.

Discussion

The purpose of this comprehensive review article is to inform scientists, clinicians, engineers, and hardware professionals of the state-of-the-art in MRgRFHT devices to potentially accelerate technical and clinical investigations in this space. Our literature search shows that an increasing number of groups are investigating approaches to apply HT under MR guidance (Figure 2). Although most of the devices developed (Table 1) have not been evaluated in the clinic, multiple *in vivo* experiments demonstrated the maturity of MRT for clinical applications. Especially, for the BSD and MAPA applicators, the results of clinical validations show a high correlation between MR-derived temperature and invasive probe measurements. However, these results were obtained in anatomical regions where MR signals were minimally affected by motion, i.e., distal from tissues impacted by moving air in intestines, cardiac, bowel, and respiratory motion. Hence, improved motion robust MR thermometry approaches for HT are still highly warranted.

In our list, 10 devices were intended for clinical use. However, only two of them were actively used in the clinic (BSD2000-3D-MRI, MAPA), and only the BSD2000-3D-MRI is commercially available. Both of these applicators operate in a 1.5 T MRI system. This is convenient since 1.5 T systems are cheaper and more available than the 3 T systems. Furthermore, it is easier to filter the high-power RF hyperthermia signals (100 MHz or 140 MHz) from the 1.5 T RF transmit/receive signals (64 MHz) compared to the 3 T RF signals (128 MHz) during simultaneous RF hyperthermia treatment and MR imaging. Dual function devices by design do not have to tackle this issue. Higher field strengths are also preferable because the Larmor frequency approaches the optimum heating frequency, which is between 150 and 300 MHz in the pelvic region and between 300 and 915 MHz for head and neck and extremities [78]. After the early feasibility studies of diffusion-based MR thermometry methods, PRFS-based MRT methods were used in all studies. Spoiled gradient echo

sequence with echo times close to the $T2^*$ of muscle tissue is commonly used for PRFS-based MRT scans [44,49,60,62,64,68]. In addition to treatment monitoring, MRT also provides unique opportunities to validate EM models with 3D measurements. Validation by MRT was only utilized for the BSD, MRlabcollar, CWA, and dual function bowtie array applicators.

The MR compatibility of complex assemblies like RF hyperthermia arrays coupled to waterbolus structures is often difficult to achieve. In addition, MR-compatible applicators are typically less efficient and controllable in comparison to the corresponding applicators outside MRI. Since MR compatibility requires the use of non-magnetic components, many off-the-shelf connectors, baluns (required to go from unbalanced coax to a balanced dipole) and matching network approaches cannot be used. The circulatory movement of water in the water bolus often generates MR image artifacts. Consequently, the efficiency and the capability to control the RF heating pattern might be compromised in MR-compatible applicator types. On the other hand, the availability of 2D/3D MRT temperature maps now provides a unique opportunity to improve and optimize the treatments. If MRT cannot be utilized to improve thermotherapies, MR-compatible applicator types will only be useful for accurate modeling of treatment setup.

Reporting of validation results

Comparing the performance of these devices is currently not straight-forward. This stems from the fact that, there is a lack of general metrics for quantitative and qualitative validation of MRgRFHT devices. In several cases, performances of devices were reported in vague terms such as 'reasonable correlations' and 'relatively comparable'. As the data in Table 1 show, different investigations reported different goals and metrics for the validation. Out of 25 clinical and pre-clinical validation experiments for 15 reviewed devices, 12 contain reports on heating ability (7 quantitative and 5 qualitative validations), 12 on MR compatibility (1 quantitative and 11 qualitative validations) and 20 on MRT accuracy (18 quantitative and 2 qualitative validations).

In our view, validation of an MR-guided RF HT device can be broken down into three distinct topics: heat focusing and steering, MR compatibility, and MRT accuracy. Based on our review, we extracted and recommended metrics for standardization of the validation (Table 2).

First, an RF HT device's ability to apply heat in a targeted manner may be characterized by minimum hot spot size, steerability of hot spots, and spatial conformality of heated regions to some desired region. Metrics to describe these qualities may be defined in terms of temperature rise or SAR. Second, the devices interaction with the MR environment, i.e., MR Safety and MR compatibility, should be assessed. The test methods for MR safety have been identified by committees [79–82] but there is currently no set of tests for MR compatibility. We recommend that a device's effect on B0 homogeneity, B1+ homogeneity, and SNR should be measured for MR compatibility assessment. To that end, image

Table 1. Table summarizes original studies on MR-guided RF HT devices.

Device	MRI insert configuration (HT-only/ dual-function)		Intended application (preclinical/clinical) and body site	MRI system Information	Validation status		Heating validation metric (Qualitative/quantitative)	MR compatibility validation metric (qualitative/ quantitative)	MRT sequence and parameters used for quantitative validation	MRT accuracy validation metric (Qualitative/quantitative)
	HT-only				Not validated versus validated (preclinical/clinical)	Preclinical: cylindrical and elliptical phantoms				
BSD2000-3D-MRI: 12 dipole pairs (100MHz) [40,42-47]	HT-only		Clinical – lower extremities and the pelvis	1.5T Body Coil RX/TX chain Simultaneous heating and imaging	Preclinical: cylindrical and elliptical phantoms	Quant.: Mean $T_{\text{increase,max}} = 5.9 \pm 0.4^{\circ}\text{C}$, Mean_steering error = $0.4 \pm 0.2\text{ cm}$ [44]	Quant.: Mean $T_{\text{increase,max}} = 5.9 \pm 0.4^{\circ}\text{C}$, Mean_steering error = $0.4 \pm 0.2\text{ cm}$ [44]	Not reported	SPGR sequence with TR: 600 ms TE: 20 ms FA:50 Reso: not reported [42] SPGR sequence with TR: 600 ms TE: 5, 20 ms FA:50 $3.9 \times 3.9 \times 10\text{ mm}^3$ [40] SPGR sequence with TR: 750 ms TE: 4, 20 ms FA:50 Reso: $3.9 \times 3.9 \times 10\text{ mm}^3$ [43] SPGR sequence with TR: 600 ms TE: 20 ms FA:50 Reso: $3.9 \times 3.9 \times 10\text{ mm}^3$ [45]	Quant.: $\Delta T_{\text{ave}} = \pm 0.4^{\circ}\text{C}$ [42] $T_{\text{Resolution}} = \pm 0.5-1^{\circ}\text{C}$ [40] $\Delta S_{\text{ARave}} < 10\%$ [43]
MAPA: 4 flared pairs (140MHz) [48-50]	HT-only		Clinical – extremities	1.5T Head Coil RX – Body Coil RX/TX chain Simultaneous heating and imaging	Clinical: 24 patients: 15 \times rectum/bladder [46] Preclinical: cylindrical phantom [48]	Qual.: $T_{\text{ave,MRT}}$ of the tumor is a useful variable to evaluate the quality and effectivity of treatments [46]	Qual.: MRqHT is feasible. [45,46]	Not reported	SPGR sequence with TR: 600 ms TE: 20 ms FA:50 Reso: $3.9 \times 3.9 \times 10\text{ mm}^3$ [45]	Quant.: $p = 0.04$: MRT _{ave,tumor} versus clinical response [45]
	HT-only		Preclinical – H&N	1.5T Body Coil RX/TX chain Sequential heating and imaging	Preclinical: cylindrical phantom	Quant.: $T_{\text{increase,max}} = 4.5^{\circ}\text{C}$ [53] $R^2 = 0.76$: Thermal distribution size and shape in MRT versus simulations [52] Qual: capability of the focused heating was confirmed [53]	Not reported	Not reported	SPGR sequence with TR: 34 ms TE: 20 ms FA:50 Reso: $0.9 \times 0.9 \times 10\text{ mm}^3$ [49,50]	$R^2 = 0.96$: MRT versus conventional invasive thermometry ^a [45] Quant: $\Delta T_{\text{ave}} < 0.2^{\circ}\text{C}$, $R^2 = 0.998$ [49] Quant: $R^2 = 0.84$ $\Delta T_{\text{ave, tumor}} < 0.62^{\circ}\text{C}$
MRlabCollar (434 MHz) [52,53,55]	HT-only		Clinical – brain (nanoparticle)	3T Body Coil RX/TX chain Sequential heating and imaging	Preclinical: cylindrical phantom	Quant.: $T_{\text{increase,max}} = 4.5^{\circ}\text{C}$ [53] $R^2 = 0.76$: Thermal distribution size and shape in MRT versus simulations [52] Qual: capability of the focused heating was confirmed [53]	Not reported	Not reported	SPGR sequence with TR: 110 ms TE: 10 ms FA:60 Reso: $1.6 \times 1.6 \times 1.6\text{ slice thickness not reported mm}^3$ [57,58]	Quant: $\Delta T_{\text{ave}} < 0.14^{\circ}\text{C}$, $\Delta T_{\text{max}} = 0.22^{\circ}\text{C}$ [55]
MRCollar (434 MHz) [56]	HT-only		Clinical – H&N	1.5T Not reported	Preclinical: reduced scale setup (continuation of MRlabcollar)	Not reported	Not reported	Not reported	Not reported	Not reported
RF capacitive (26 MHz) [57,58]	HT-only		Clinical – deep seated tumor	4.7T Body Coil RX/TX chain Simultaneous heating and imaging	Preclinical: cylindrical phantom	Qual: ability to control of the position of the focal point [73]	Not reported	Not reported	GRASS sequence with TR: 160 ms TE: 20 ms FA:40 Reso: $2 \times 2 \times 10\text{ mm}^3$ [60]	Quant: $\Delta T_{\text{ave}} = \pm 1^{\circ}\text{C}$, $\Delta T_{\text{SD}} = 0.4^{\circ}\text{C}$ [60]
APA (915 MHz) [73]	HT-only		Clinical – deep-seated pelvic and abdominal	3T Body Coil RX/TX chain Sequential heating and imaging	Preclinical: cuboid phantom	Not reported	Not reported	Not reported	GRASS sequence with TR: 160 ms TE: 20 ms FA:40 Reso: $2 \times 2 \times 10\text{ mm}^3$ [60]	Quant: $\Delta T_{\text{ave}} = \pm 1^{\circ}\text{C}$, $\Delta T_{\text{SD}} = 0.4^{\circ}\text{C}$ [60]

(continued)

Table 1. Continued.

Device	MRI insert configuration (HT-only/ dual-function)	Intended application (preclinical/clinical) and body site	MRI system Information	Validation status (preclinical/clinical)	Heating validation metric (Qualitative/quantitative)	MR compatibility validation metric (qualitative/ quantitative)	MRT sequence and parameters used for quantitative validation	MRT accuracy validation metric (Qualitative/quantitative)
CWA (100 MHz) [61,62]	HT-only	Clinical – pelvis and abdomen	1.5T Body Coil RX/TX chain Simultaneous heating and imaging	Preclinical: cylindrical phantom Not validated versus validated (preclinical/clinical)	Qual.: good ability of field pattern steering [61,62]	Qual.: MR-compatibility has been verified in preliminary tests [61]	SPGR sequence with TR: 600 ms TE: 20 ms FA:50 3.9 × 3.9 × 10 mm ³ [62]	Quant.: $\Delta T_{ave} = 0.45^{\circ}\text{C}$ [62]
Intravascular MRI guidewire (180 MHz) [67]	HT-only	Clinical – vessel wall	1.5T Body Coil TX chain/ Intravascular MRI guidewire RX Simultaneous heating and imaging	Preclinical: cylindrical phantom	Not reported	Qual.: The SNR profile was comparable to the pattern of simulated RF power distribution	SPGR sequence with TR: 68 ms TE: 15 ms FA:30 0.9 × 0.9 × 8 mm ³	Qual.: The simulated RF power distribution was comparable to that of MRT Quant.: $\Delta T_{SD} = 1.2^{\circ}\text{C}$
Slot & Dipole-type (2.45 GHz) [68]	HT-only	Preclinical – animal thigh muscle	7T Body Coil RX/TX chain Sequential heating and imaging	Preclinical: cuboid phantom 10 male rabbits: thigh muscle In 6 rabbits: VX2 tumor cells were inserted	Not reported Not reported Quant.: $T_{increase, max} \approx 7^{\circ}\text{C}$	Not reported	SPGR sequence with TR: 20 ms TE: 8 ms FA:20 1.2 × 1.2 × 3 mm ³	Quant.: $\Delta T_{SD} = +0.318/-0.339^{\circ}\text{C}$ $\Delta T_{SD} = +0.693/-0.661^{\circ}\text{C}$ $\Delta T_{SD} = +0.564/-0.526^{\circ}\text{C}$
Coaxial-type (2.45 GHz) [69]	HT-only	Preclinical – local tumors in small animals	7T Body Coil RX/TX chain Simultaneous heating and imaging	Preclinical: cylindrical phantom 2 experimental mice with implanted tumors	Not reported Quant.: $T_{increase} \geq 3^{\circ}\text{C}$	Not reported	SPGR sequence with TR: 40 ms TE: 4 ms FA:25 2.3 × 2.3 × 1 mm ³	Quant.: $\Delta T_{max} \leq \pm 0.6^{\circ}\text{C}$
Hexagonal flared-type (130 MHz) [63–66]	HT-only	Preclinical – whole body	1.5T Body Coil RX/TX chain Simultaneous heating and imaging	Preclinical: cylindrical phantom 2 canines: brain and muscle	Not reported Qual.: ability to create a small heating focus (<1cm ³). Satisfactory agreement between simulated versus MRT distribution	Qual.: Simultaneous heating and imaging without deterioration of SNR [63]	SPGR sequence with TR: 34 ms TE: 20 ms FA:25 0.6 × 0.6 × 4 mm ³	Quant.: $\Delta T_{ave} = 0.92^{\circ}\text{C}$ $T_{RMS} = 1.23^{\circ}\text{C}$ [63] $T_{resolution} = 0.22^{\circ}\text{C}$ [64] $T_{resolution} = 0.6^{\circ}\text{C}$ [64]
Yagi-Uda-based (2.45 GHz) [70,72]	HT-only	Preclinical – superficial tumors in small animals (murine)	7T Body Coil RX/TX chain Simultaneous heating and imaging	4 mice: tumor on leg [73]	Quant.: $T_{increase} = 7^{\circ}\text{C}$	Qual.: The applicator is MR-compatible. No disturbances are visible in the area of interest	Not reported	Not reported
Electronic switching: Coil/C-shaped dipole (Larmor freq.) [75]	Dual-function	Preclinical – not mentioned	3T Body Coil RX/TX chain Sequential heating and imaging	Preclinical: cylindrical phantom	Qual.: Ability for steerable heating. Repeatable heating patterns in subsequent experiments.	Not reported	SPGR sequence with TR: 100 ms TE: 12 ms FA:35 Reso: 3.75 × 3.75 × 10 mm ³	Quant.: $T_{increase, max} \approx 4.3^{\circ}\text{C}$ in 45 min
Thermal MR: Bow-tie dipoles (Larmor freq.) [76,77]	Dual-function	Preclinical – not mentioned	7T Body Coil RX/TX chain Sequential heating and imaging	Preclinical: cylindrical phantom	Qual.: ability to generate and steer deep-seated temperature focus [76] Quant.: $T_{increase} \sim 11^{\circ}\text{C}$ center of a head sized phantom [77]	Not reported	Not reported	Not reported
Statistics of preclinical devices	5 × HT only 2 × Dual-function	7 × Preclinical devices		12 × Preclinical validations	5 × Quant 2 × only Qual 5 × Not reported	0 × Quant 4 × only Qual 8 × Not reported	5 × SPGR 2 × GRE	8 × Quant 1 × only Qual 3 × Not reported

(continued)

Table 1. Continued.

Device	MRI insert configuration (HT-only/ dual-function)	Intended application (preclinical/clinical) and body site	MRI system Information	Validation status (preclinical/clinical)	Heating validation metric (Qualitative/quantitative)	MR compatibility validation metric (qualitative/quantitative)	MRT sequence and parameters used for quantitative validation	MRT accuracy validation metric (Qualitative/quantitative)
Statistics of clinical devices	8 × HT only	8 × Clinical devices		9 × Preclinical validations Not validated versus validated (preclinical/clinical)	2 × Quant 2 × only Qual 5 × Not reported 0 × Quant 1 × only Qual 3 × Not reported	0 × Quant 5 × only Qual 4 × Not reported 1 × Quant 2 × only Qual 1 × Not reported	6 × SPGR 2 × GRE 1 × GRASS 2 × SPGR 2 × GRE	6 × Quant 1 × only Qual 2 × Not reported 4 × Quant 0 × only Qual 0 × Not reported

Note that in view of clarity, for each parameter, only the best achieved data is summarized in this table. Unless stated, all reported accuracies were measured versus fiber-optic temperature probe. R^2 : correlation coefficient, ΔT_{ave} : average temperature error, ΔT_{SD} : standard deviation of temperature error, ΔT_{max} : maximum temperature error, $T_{resolution}$: thermal resolution, SAR: specific absorption rate, SNR: signal to noise ratio. The statistics at the end of the table are highlighted with gray to distinguish that area from the devices.

^aThe accuracy of the MRT was measured against Bowman probes (high-impedance thermistors).

SNR [83–86] and geometric distortions [87,88] should be quantified. Furthermore, sufficient decoupling between MRI RF frequency and HT RF frequency (and its harmonics and parasitic frequencies) needs to be demonstrated. Lastly, the validation of MR thermometry should be quantified as the difference between the MR-derived versus invasive measured temperature increase for various probe sensor points based on National Institute of Standards and Technology (NIST). For experiments that involve the use of phantoms, the phantom's dimensions, shape, material, and probe locations should be reported. In the case of *in vivo* experiments, the number of subjects, region of interest, pathology type, and probe insertion locations should be reported, where applicable. For all MRI-based measurements, the MRI pulse sequence type, scan parameters (e.g., echo time, repetition time, flip angle, matrix size, slice thickness, field of view, total acquisition time, etc.) should be reported.

The further development of MRgRFHT

Future work will aim to improve thermotherapy delivery performance by enabling more accurate temperature monitoring with dedicated sequences and post processing techniques that mitigate artifacts, e.g., motion. Accurate temperature monitoring enables to adjust the SAR for better targeting the heat into the tumor area. New hardware solutions are urgently needed to simplify and reduce equipment profile to increase patient access to MR-guided RF HT in the clinic, e.g., low-profile liquid bolus for permittivity matching and cooling, and dual-function integrated MR-RF HT applicators for improved SNR in MR thermometry.

An excellent potential of using a single integrated antenna array structure for dual-function devices has been demonstrated in the literature. However, that approach is hampered by (1) the need for sequential heating and imaging, and (2) potentially contradicting requirements in terms of frequency and coil/antenna design. Decoupled devices have the benefit that different frequencies can be used for imaging and heating, which enables (1) simultaneous operation and (2) the possibility of exploiting optimal heating frequencies regardless of the imaging frequency. Another benefit of the latter approach is that it allows RF HT to be applied on the most commonly available MRI field strength in the clinic (1.5 T) today, which can potentially increase patients' access to RF HT and lower operational costs. Hence, accessibility of electronic switching and thermal MR approaches are strongly dependent on the progress in the clinical availability of scanners based on 3 T, 7 T or beyond.

The ability to quickly reconfigure the setup of an MRI scanner from RF hyperthermia treatment to standard diagnostic imaging mode, and vice versa, is also important in a clinical setting. This is especially if the clinic aims to maximize patient throughput on the scanner, regardless of whether it is used for therapy or diagnostic imaging. Thus, the RF hyperthermia equipment and associated software needs to be configured such that a quick change between diagnostic and interventional modes of an MRI scanner can

Table 2. Summary of proposed validation stages and metrics for standardization of the validation of MRgHT devices.

Topic	Sub-topic	Quantification metric
Heating ability	Focusing	Option 1: T_{target} , increase Option 2: SAR_{max} for 1 W input power Option 3: 50% iso-SAR contour
	Focus steering	Option 1: relocation of maximum heating point (mm) Option 2: relocation of center of the 50% iso-SAR contour (mm)
Compatibility	B0	No standardized metrics were found in literature. Proposal: average and maximum $\Delta B0$ changes with/without the RF HT device present
	B1+	No standardized metrics were found in literature. Proposal: average and maximum $\Delta B1+$ changes with/without the RF HT device present
	Decoupling	No standardized metrics were found in literature. Proposal: Option 1: Coupling between the systems (S-matrix). Option 2: Image quality degradation metrics during contemporaneous operation of MRI and RF HT
MRT accuracy	Image noise	Image signal to noise ratio (SNR)
	Geometric distortion	DICE score, normalized cross-correlation of landmarks in calibration phantoms
	ΔT Accuracy	Root mean squared error (RMSE)
	ΔT bias and precision	Mean error (ME) and Standard error (SE)
	Correlation	Coefficient of determination (R^2) and probability (p -value)

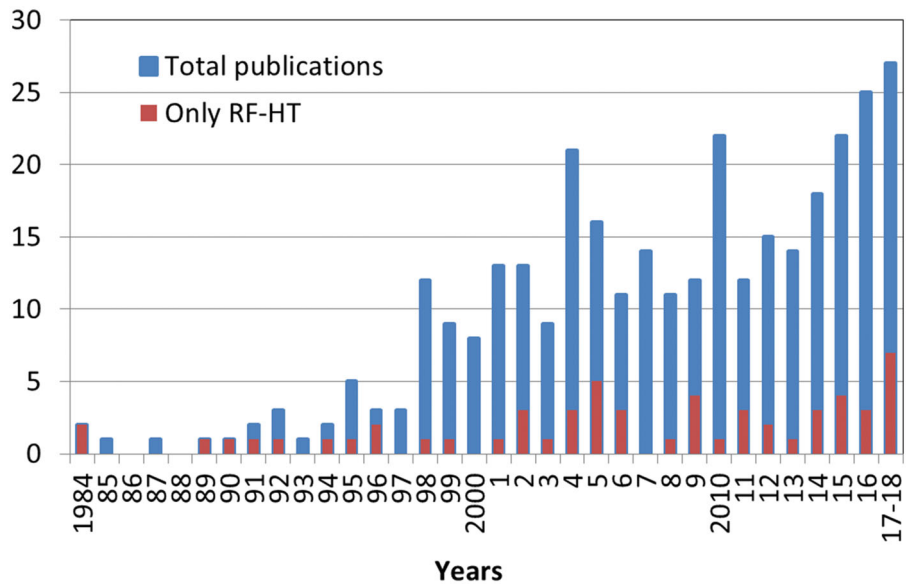


Figure 2. The number of publications over years after applying the search string and exclusion criterion 1 provided in the text (Material and methods). An increased number of publications on MR-guided RF HT (red bars) can be seen after 2001 (development of the BSD2000-3D-MRI) and after 2014 (development of the MRlabcollar and Thermal MRI).

be made. This may involve dedicated scanner tables and software for diagnostic versus therapy modes.

The current clinical application of MR guided RF hyperthermia is strongly hampered by motion, heterogeneities, clips, and physiological changes (bladder filling, perfusion, swelling). The major problem with the PRFS (used in most cases) is the strong disturbance by motion and heterogeneities. Other MR parameters ($T1$ or $T2$) might be better suitable since these are less sensitive to motion, and motion correction techniques like gating could be applied. Note that many of these techniques are studied in the context of thermal ablation [89–91], but application for the range of 40–44 °C still has to be studied. For all methods, increasing SNR is highly warranted since this allows for faster scanning and/or more accurate measurements. We foresee that clinical

translation of the novel applicator approaches reported in this review will provide big steps toward achieving sufficient SNR as groundwork for accurate MRT in the clinic. This, in turn, will aid in the development of more precise heating devices and truly, i.e., MRT feedback controlled, application of MRgRFHT.

Conclusion

In conclusion, on-line noninvasive 3D MR thermometry (MRT) offers very valuable information about the tumor and normal tissues to improve treatment planning, treatment monitoring and assessment of treatment effectiveness. The results obtained thus far from the MR-guided RF HT devices

described are very promising, and MRT during RF HT treatment has been demonstrated to be feasible in selected cases. Still, improvements are highly warranted to enable MRT guided treatment and treatment optimization in more anatomical locations with greater robustness to motion-induced artifacts. Technical advances during recent years may provide promising solutions to overcome many of the technical obstacles such as poor temperature measurement accuracy, low temporal resolution and low imaging SNR. Unfortunately, it is difficult to truly compare the advances since very little standardization was observed in the ongoing work on device validation. In this paper, we, therefore, list currently used metrics and propose new ones in case of gaps for experimental validation of such devices. We believe that homogeneous reporting of validation results will help selecting the best approach for all clinical scenarios. Hence, this paper will form a major drive for clinical implementation of new MR hyperthermia technologies and, hence, will reduce one roadblock for achieving spatially and biologically selective exploitation of the pallet of hyperthermia benefits.

Disclosure statement

No potential conflict of interest was reported by the authors.

ORCID

Kemal Sumser  <http://orcid.org/0000-0002-6695-2659>

References

- [1] Dewhurst MW, Vujaskovic Z, Jones E, et al. Re-setting the biologic rationale for thermal therapy. *Int J Hyperthermia*. 2005;21:779–790.
- [2] Lee ER. Electromagnetic superficial heating technology. In: Seegenschmiedt MH, editor. *Thermoradiotherapy and thermochemotherapy*. Berlin: Springer Verlag; 1995. p. 193–217.
- [3] Wust P, Seebass M, Nadobny J, Felix R. Electromagnetic deep heating technology. In: Seegenschmiedt MH, Vernon CC, editors. *Principles and practice of thermoradiotherapy and thermochemotherapy*. Berlin: Springer Verlag; 1995. p. 219–251.
- [4] Datta NR, Puric E, Klingbiel D, et al. Hyperthermia and radiation therapy in locoregional recurrent breast cancers: a systematic review and meta-analysis. *Int J Radiat Oncol Biol Phys*. 2016;94:1073–1087.
- [5] Datta NR, Rogers S, Klingbiel D, et al. Hyperthermia and radiotherapy with or without chemotherapy in locally advanced cervical cancer: a systematic review with conventional and network meta-analyses. *Int J Hyperthermia*. 2016;32:809–821.
- [6] Datta NR, Rogers S, Ordóñez SG, et al. Hyperthermia and radiotherapy in the management of head and neck cancers: a systematic review and meta-analysis. *Int J Hyperthermia*. 2016;32:31–40.
- [7] Oleson JR, Dewhurst MW, Harrelson JM, et al. Tumor temperature distributions predict hyperthermia effect. *Int J Radiat Oncol Biol Phys*. 1989;16:559–570.
- [8] Issels RD, Prenninger SW, Nagele A, et al. Ifosfamide plus etoposide combined with regional hyperthermia in patients with locally advanced sarcomas: a phase II study. *JCO*. 1990;8:1818–1829.
- [9] Leopold KA, Dewhurst MW, Samulski TV, et al. Cumulative minutes with T90 greater than tempindex is predictive of response of superficial malignancies to hyperthermia and radiation. *Int J Radiat Oncol Biol Phys*. 1993;25:841–847.
- [10] Hildebrandt B. The cellular and molecular basis of hyperthermia. *Crit Rev Oncol/Hematol*. 2002;43:33–56.
- [11] Cihoric N, Tsikkinis A, van Rhoon G, et al. Hyperthermia-related clinical trials on cancer treatment within the ClinicalTrials.gov registry. *Int J Hyperthermia*. 2015;31:609–614.
- [12] Issels RD, Lindner LH, Verweij J, et al; for the European Organization for the Research and Treatment of Cancer-Soft Tissue and Bone Sarcoma Group and the European Society for Hyperthermic Oncology. Effect of neoadjuvant chemotherapy plus regional hyperthermia on long-term outcomes among patients with localized high-risk soft tissue sarcoma: the EORTC 62961-ESHO 95 randomized clinical trial. *JAMA Oncol*. 2018;4:483–492.
- [13] Issels RD, Lindner LH, Verweij J, et al. Neo-adjuvant chemotherapy alone or with regional hyperthermia for localised high-risk soft-tissue sarcoma: a randomised phase 3 multicentre study. *Lancet Oncol*. 2010;11:561–570.
- [14] Huilgol NG, Gupta S, Sridhar CR. Hyperthermia with radiation in the treatment of locally advanced head and neck cancer: a report of randomized trial. *J Can Res Ther*. 2010;6:492.
- [15] van der Zee J, González D, van Rhoon GC, et al. Dutch Deep Hyperthermia Group. Comparison of radiotherapy alone with radiotherapy plus hyperthermia in locally advanced pelvic tumours: a prospective, randomised, multicentre trial. *Lancet*. 2000;355:1119–1125.
- [16] Murbach M, Neufeld E, Capstick M, et al. Thermal tissue damage model analyzed for different whole-body SAR and scan durations for standard MR body coils. *Magn Reson Med*. 2014;71:421–431.
- [17] Vaupel PW, Kelleher DK. Pathophysiological and vascular characteristics of tumours and their importance for hyperthermia: heterogeneity is the key issue. *Int J Hyperthermia*. 2010;26:211–223.
- [18] Vujaskovic Z, Song CW. Physiological mechanisms underlying heat-induced radiosensitization. *Int J Hyperthermia*. 2004;20:163–174.
- [19] Song CW, Lokshina A, Rhee JG, et al. Implication of blood flow in hyperthermic treatment of tumors. *IEEE Trans Biomed Eng*. 1984; BME-31:9–16.
- [20] Winter L, Oberacker E, Paul K, et al. Magnetic resonance thermometry: methodology, pitfalls and practical solutions. *Int J Hyperthermia*. 2016;32:63–75.
- [21] Odéen H, Parker DL. Magnetic resonance thermometry and its biological applications – physical principles and practical considerations. *Prog Nuclear Magn Reson Spectrosc*. 2019;110:34–61.
- [22] Van Rhoon GC, Wust P. Introduction: non-invasive thermometry for thermotherapy. *Int J Hyperthermia*. 2005;21:489–495.
- [23] Bowman RR. A probe for measuring temperature in radio-frequency-heated material. *IEEE Trans Microwave Theory Techn*. 1976;24:43–45.
- [24] Christensen DA. A new nonperturbing temperature probe using semiconductor band edge shift. *J Bioeng*. 1977;1:541–545.
- [25] Wickersheim KA, Alves RB. Recent advances in optical-temperature measurement. *Ind Res Dev*. 1979;21:82–89.
- [26] Van Der Zee J, Peer-Valstar JN, Rietveld PJ, et al. Practical limitations of interstitial thermometry during deep hyperthermia. *Int J Radiat Oncol Biol Phys*. 1998;40:1205–1212.
- [27] Wust P, Gellermann J, Harder C, et al. Rationale for using invasive thermometry for regional hyperthermia of pelvic tumors. *Int J Radiat Oncol Biol Phys*. 1998;41:1129–1137.
- [28] Parker DL, Smith V, Sheldon P, et al. Temperature distribution measurements in two-dimensional NMR imaging. *Med Phys*. 1983;10:321–325.
- [29] De Poorter J, et al. The proton-resonance-frequency-shift method compared with molecular diffusion for quantitative measurement of two-dimensional time-dependent temperature distribution in a phantom. *J Magn Reson Ser B*. 1994;103:234–241.
- [30] Ishihara Y, Calderon A, Watanabe H, et al. A precise and fast temperature mapping using water proton chemical shift. *Magn Reson Med*. 1995;34:814–823.
- [31] Poorter JD. Noninvasive mri thermometry with the proton-resonance frequency method - study of susceptibility effects. *Magn Reson Med*. 1995;34:359–367.

- [32] Le Bihan D, Delannoy J, Levin RL. Temperature mapping with MR imaging of molecular diffusion: application to hyperthermia. *Radiology*. 1989;171:853–857.
- [33] Lüdemann L, Włodarczyk W, Nadobny J, et al. Non-invasive magnetic resonance thermography during regional hyperthermia. *Int J Hyperthermia*. 2010;26:273–282.
- [34] Rieke V, Pauly KB. MR thermometry. *J Magn Reson Imaging*. 2008;27:376–390.
- [35] Baron P, Ries M, Deckers R, et al. In vivo T2-based MR thermometry in adipose tissue layers for high-intensity focused ultrasound near-field monitoring. *Magn Reson Med*. 2014;72:1057–1064.
- [36] McDannold N. Quantitative MRI-based temperature mapping based on the proton resonant frequency shift: review of validation studies. *Int J Hyperthermia*. 2005;21:533–546.
- [37] Hindman JC. Proton resonance shift of water in the gas and liquid states. *J Chem Phys*. 1966;44:4582–4592.
- [38] Vigen KK, Daniel BL, Pauly JM, et al. Triggered, navigated, multi-baseline method for proton resonance frequency temperature mapping with respiratory motion. *Magn Reson Med*. 2003;50:1003–1010.
- [39] Rieke V, Vigen KK, Sommer G, et al. Referenceless PRF shift thermometry. *Magn Reson Med*. 2004;51:1223–1231.
- [40] Gellermann J, Włodarczyk W, Feussner A, et al. Methods and potentials of magnetic resonance imaging for monitoring radiofrequency hyperthermia in a hybrid system. *Int J Hyperthermia*. 2005;21:497–513.
- [41] Grissom WA, Rieke V, Holbrook AB, et al. Hybrid referenceless and multibaseline subtraction MR thermometry for monitoring thermal therapies in moving organs. *Med Phys*. 2010;37:5014–5026.
- [42] Gellermann J, Włodarczyk W, Ganter H, et al. A practical approach to thermography in a hyperthermia/magnetic resonance hybrid system: validation in a heterogeneous phantom. *Int J Radiat Oncol Biol Phys*. 2005;61:267–277.
- [43] Gellermann J, Weihrach M, Cho CH, et al. Comparison of MR-thermography and planning calculations in phantoms. *Med Phys*. 2006;33:3912–3920.
- [44] Mulder HT, Curto S, Paulides MM, et al. Systematic quality assurance of the BSD2000-3D MR-compatible hyperthermia applicator performance using MR temperature imaging. *Int J Hyperthermia*. 2018;35:305–313.
- [45] Gellermann J, Hildebrandt B, Issels R, et al. Noninvasive magnetic resonance thermography of soft tissue sarcomas during regional hyperthermia: correlation with response and direct thermometry. *Cancer*. 2006;107:1373–1382.
- [46] Gellermann J, Włodarczyk W, Hildebrandt B, et al. Noninvasive magnetic resonance thermography of recurrent rectal carcinoma in a 1.5 tesla hybrid system. *Cancer Res*. 2005;65:5872–5880.
- [47] Weihrach M, Wust P, Weiser M, et al. Adaptation of antenna profiles for control of MR guided hyperthermia (HT) in a hybrid MR-HT system. *Med Phys*. 2007;34:4717–4725.
- [48] Delannoy J, LeBihan D, Hoult DI, et al. Hyperthermia system combined with a magnetic resonance imaging unit. *Med Phys*. 1990;17:855–860.
- [49] Delannoy J, Chen C-N, Turner R, et al. Noninvasive temperature imaging using diffusion MRI. *Magn Reson Med*. 1991;19:333–339.
- [50] Carter DL, MacFall JR, Clegg ST, et al. Magnetic resonance thermometry during hyperthermia for human high-grade sarcoma. *Int J Radiat Oncol Biol Phys*. 1998;40:815–822.
- [51] Craciunescu OI, Stauffer PR, Soher BJ, et al. Accuracy of real time noninvasive temperature measurements using magnetic resonance thermal imaging in patients treated for high grade extremity soft tissue sarcomas. *Med Phys*. 2009;36:4848–4858.
- [52] Numan WCM, Hofstetter LW, Kotek G, et al. Exploration of MR-guided head and neck hyperthermia by phantom testing of a modified prototype applicator for use with proton resonance frequency shift thermometry. *Int J Hyperthermia*. 2014;30:184–191.
- [53] Paulides MM, Bakker JF, Hofstetter LW, et al. Laboratory prototype for experimental validation of MR-guided radiofrequency head and neck hyperthermia. *Phys Med Biol*. 2014;59:2139–2154.
- [54] Paulides MM, Bakker JF, van Rhoon GC. Electromagnetic head-and-neck hyperthermia applicator: experimental phantom verification and FDTD model. *Int J Radiat Oncol Biol Phys*. 2007;68:612–620.
- [55] Tarasek MR, Pellicer R, Hofstetter LW, et al. Validation of MR thermometry: method for temperature probe sensor registration accuracy in head and neck phantoms. *Int J Hyperthermia*. 2014;30:142–149.
- [56] Paulides MM, Drizdal T, Van Rhoon GC, et al. Novel applicator design for MR guided RF hyperthermia in head and neck cancers: heating performance and RF coupling. Paris (France): International Society for Magnetic Resonance in Medicine (ISMRM); 2018.
- [57] Kim KS, Lee SY. Nanoparticle-mediated radiofrequency capacitive hyperthermia: a phantom study with magnetic resonance thermometry. *Int J Hyperthermia*. 2015;31:831–839.
- [58] Kim KS, Hernandez D, Lee SY. Time-multiplexed two-channel capacitive radiofrequency hyperthermia with nanoparticle mediation. *Biomed Eng Online*. 2015;14:95.
- [59] Hernandez D, Kim KS, Michel E, et al. Correction of B0 drift effects in magnetic resonance thermometry using magnetic field monitoring technique. *Concepts Magn Reson*. 2016;46B:81–89.
- [60] Hoffmann W, Rhein KH, Wojcik F, et al. Performance and use of current sheet antennae for RF-hyperthermia of a phantom monitored by 3 tesla MR-thermography. *Int J Hyperthermia*. 2002;18:454–471.
- [61] Nadobny J, Włodarczyk W, Westhoff L, et al. Development and evaluation of a three-dimensional hyperthermia applicator with water-coated antennas (WACOA). *Med Phys*. 2003;30:2052–2064.
- [62] Nadobny J, Włodarczyk W, Westhoff L, et al. A clinical water-coated antenna applicator for MR-controlled deep-body hyperthermia: a comparison of calculated and measured 3-D temperature data sets. *Ieee Trans Biomed Eng*. 2005;52:505–519.
- [63] Samulski TV, MacFall J, Zhang Y, et al. Non-invasive thermometry using magnetic resonance diffusion imaging: potential for application in hyperthermic oncology. *Int J Hyperthermia*. 1992;8:819–829.
- [64] MacFall JR, Prescott DM, Charles HC, et al. 1H MRI phase thermometry in vivo in canine brain, muscle, and tumor tissue. *Med Phys*. 1996;23:1775–1782.
- [65] MacFall J, Prescott DM, Fullar E, et al. Temperature dependence of canine brain tissue diffusion coefficient measured in vivo with magnetic resonance echo-planar imaging. *Int J Hyperthermia*. 1995;11:73–86.
- [66] Samulski TV, Clegg ST, Das S, et al. Application of new technology in clinical hyperthermia. *Int J Hyperthermia*. 1994;10:389–394.
- [67] Qiu B, El-Sharkawy A-M, Paliwal V, et al. Simultaneous radiofrequency (RF) heating and magnetic resonance (MR) thermal mapping using an intravascular MR imaging/RF heating system. *Magn Reson Med*. 2005;54:226–230.
- [68] Demura K, Morikawa S, Murakami K, et al. An easy-to-use microwave hyperthermia system combined with spatially resolved MR temperature maps: phantom and animal studies. *J Surg Res*. 2006;135:179–186.
- [69] Curto S, Faridi P, Shrestha TB, et al. An integrated platform for small-animal hyperthermia investigations under ultra-high-field MRI guidance. *Int J Hyperthermia*. 2018;34:341–351.
- [70] Raaijmakers EAL, Mestrom RMC, Sumser K, et al. An MR-compatible antenna and application in a murine superficial hyperthermia applicator. *Int J Hyperthermia*. 2018;34:697–703.
- [71] Paulides MM, Mestrom RMC, Salim G, et al. A printed Yagi-Uda antenna for application in magnetic resonance thermometry guided microwave hyperthermia applicators. *Phys Med Biol*. 2017;62:1831–1847.
- [72] Sumser K, Geerman A, Haack J, et al. Development and in vivo validation of an MRCompatible temperature controllable superficial hyperthermia applicator for small animal studies. *Proceedings of the 1st World Conference on Biomedical Applications of Electromagnetic Fields (EMF-Med)*; 2018 Sep 10–13; Split, Croatia. IEEE; 2018.

- [73] Kowalski ME, Behnia B, Webb AG, et al. Optimization of electromagnetic phased-arrays for hyperthermia via magnetic resonance temperature estimation. *IEEE Trans Biomed Eng.* 2002;49: 1229–1241.
- [74] Kowalski ME, Jin JM. Model-based optimization of phased arrays for electromagnetic hyperthermia. *IEEE Trans Microwave Theory Techn.* 2004;52:1964–1977.
- [75] Yeo D YX, Wu J, Hofstetter LW, et al. Investigation of a dual-function applicator for RF hyperthermia and MRI. Aarhus (Denmark): European Society for Hyperthermia Oncology (ESHO); 2011.
- [76] Winter L, Özerdem C, Hoffmann W, et al. Design and evaluation of a hybrid radiofrequency applicator for magnetic resonance imaging and RF induced hyperthermia: electromagnetic field simulations up to 14.0 Tesla and Proof-of-Concept at 7.0 Tesla. *PLoS One.* 2013;8:e61661.
- [77] Winter L, Oezerdem C, Hoffmann W, et al. Thermal magnetic resonance: physics considerations and electromagnetic field simulations up to 23.5 Tesla (1GHz). *Radiat Oncol.* 2015;10:201.
- [78] Guérin B, Villena JF, Polimeridis AG, et al. Computation of ultimate SAR amplification factors for radiofrequency hyperthermia in non-uniform body models: impact of frequency and tumour location. *Int J Hyperthermia.* 2018;34:87–100.
- [79] ASTM F2052-15, Standard Test Method for Measurement of Magnetically Induced Displacement Force on Medical Devices in the Magnetic Resonance Environment. West Conshohocken (PA): American Society for Testing and Materials International; 2015. Available from: <http://www.astm.org/cgi-bin/resolver.cgi?F2052-15>
- [80] ASTM F2213-17, Standard Test Method for Measurement of Magnetically Induced Torque on Medical Devices in the Magnetic Resonance Environment. West Conshohocken (PA): ASTM International; 2017. Available from: <http://www.astm.org/cgi-bin/resolver.cgi?F2213-17>
- [81] ASTM F2182-11a, Standard Test Method for Measurement of Radio Frequency Induced Heating On or Near Passive Implants During Magnetic Resonance Imaging. West Conshohocken (PA): ASTM International; 2011. Available from: <http://www.astm.org/cgi-bin/resolver.cgi?F2182-11a>
- [82] ISO. ISO/TS 10974:2018 Assessment of the safety of magnetic resonance imaging for patients with an active implantable medical device. 2018.
- [83] Dietrich O, Raya JG, Reeder SB, et al. Measurement of signal-to-noise ratios in MR images: influence of multichannel coils, parallel imaging, and reconstruction filters. *J Magn Reson Imaging.* 2007; 26:375–385.
- [84] Sijbers J, den Dekker AJ, Van Audekerke J, et al. Estimation of the noise in magnitude MR images. *Magn Reson Imaging.* 1998;16: 87–90.
- [85] Reeder SB, Wintersperger BJ, Dietrich O, et al. Practical approaches to the evaluation of signal-to-noise ratio performance with parallel imaging: application with cardiac imaging and a 32-channel cardiac coil. *Magn Reson Med.* 2005;54:748–754.
- [86] Kellman P, McVeigh ER. Image reconstruction in SNR units: a general method for SNR measurement. *Magn Reson Med.* 2005;54: 1439–1447.
- [87] Jafar M, Jafar YM, Dean C, et al. Assessment of geometric distortion in six clinical scanners using a 3D-printed grid phantom. *J Imaging.* 2017;3:28.
- [88] Wang D, Doddrell DM. Geometric distortion in structural magnetic resonance imaging. *CMIR.* 2005;1:49–60.
- [89] Tan J, Mougenot C, Pichardo S, et al. Motion compensation using principal component analysis and projection onto dipole fields for abdominal magnetic resonance thermometry. *Magn Reson Med.* 2019;81:195–207.
- [90] de Senneville BD, Mougenot C, Quesson B, et al. MR thermometry for monitoring tumor ablation. *Eur Radiol.* 2007;17:2401–2410.
- [91] Bour P, Ozenne V, Marquet F, et al. Evaluation of 2D simultaneous multi-slice EPI at 1.5T for MR-thermometry in presence of motion. Paris (France): International Society of Magnetic Resonance in Medicine; 2018.